

# GSORB-SLAM: Gaussian Splatting SLAM benefits from ORB features and Transmittance information

Wancai Zheng<sup>1</sup>, Xinyi Yu<sup>1,\*</sup>, Jintao Rong<sup>1</sup>, Linlin Ou<sup>1</sup>, Yan Wei<sup>1</sup>, Libo Zhou<sup>1</sup>

**Abstract**—The emergence of 3D Gaussian Splatting (3DGS) has recently sparked a renewed wave of dense visual SLAM research. However, current methods face challenges such as sensitivity to artifacts and noise, sub-optimal selection of training viewpoints, and a lack of light global optimization. In this paper, we propose a dense SLAM system that tightly couples 3DGS with ORB features. We design a joint optimization approach for robust tracking and effectively reducing the impact of noise and artifacts. This involves combining novel geometric observations, derived from accumulated transmittance, with ORB features extracted from pixel data. Furthermore, to improve mapping quality, we propose an adaptive Gaussian expansion and regularization method that enables Gaussian primitives to represent the scene compactly. This is coupled with a viewpoint selection strategy based on the hybrid graph to mitigate over-fitting effects and enhance convergence quality. Finally, our approach achieves compact and high-quality scene representations and accurate localization. GSORB-SLAM has been evaluated on different datasets, demonstrating outstanding performance. The code will be available.

## I. INTRODUCTION

Over the past two decades years, Simultaneous Localization and Mapping (SLAM) has remained a hot research topic, evolving from traditional SLAM, which focuses on improving localization accuracy, to neural radiance field (NeRF) SLAM, which provides rich scene representations. As one of the key points in fields like autonomous driving, virtual reality (VR), and embodied artificial intelligence [15], SLAM has gained increasing importance in map representation, which plays a crucial role in downstream tasks. Visual SLAM has introduced various map representations, such as point/surfel clouds [8]–[10], mesh representations [11], [12], and voxels [13], [14].

In recent years, NeRF-based novel view synthesis [16] has gained widespread popularity among researchers due to its high-fidelity construction and led to the development of numerous advanced dense neural SLAM methods. These methods have achieved impressive progress. However, because volumetric rendering expensive samples along rays in the optimization of NeRF, it cannot render full-resolution images, so the rendering results are still far from the photorealism we aspire to achieve.

This research was supported by the Baima Lake Laboratory Joint Funds of the Zhejiang Provincial Natural Science Foundation of China under Grant No. LBMHD24F030002 and the National Natural Science Foundation of China under Grant 62373329.

<sup>1</sup>All authors are with the School of Information Engineering, Zhejiang University of Technology, Hangzhou, China, 310000. {aczheng, yuxy}@zjut.edu.cn

\* Corresponding author

Excitingly, the 3D Gaussian splatting (3DGS) technique [4] has enabled high-quality, full-pixel novel view synthesis and real-time scene rendering under the standard GPU-accelerated frameworks. Consequently, several SLAM methods based on 3DGS [19]–[21] have been developed. These methods significantly improve rendering quality and achieve rendering speeds up to 100x faster compared to NeRF-based SLAM. However, pressing issues still need to be addressed, such as the Bundle Adjustment (BA) problem and sensitivity to artifacts, which leads to degraded tracking accuracy. Additionally, the lack of multi-view constraints and strong anisotropy causes Gaussians to overfit to the current viewpoint.

To address these issues, we propose a tightly coupled 3DGS and ORB feature SLAM system, called GSORB-SLAM, in the paper. For mapping, we design an adaptive extended Gaussian method that effectively identifies uninitialized Gaussian regions by combining accumulated transmittance and geometric information. This allows the system to represent the scene compactly while improving real-time performance. Additionally, to reduce overfitting caused by the lack of multi-view constraints and enhance convergence quality, we propose a viewpoint selection strategy for rendering frame (RF) that combines the overlap graph with the co-visibility graph, forming a hybrid graph. During the tracking process, we develop sparse feature points for frame-to-frame tracking, which provide an initial pose for the joint optimization of photometric and reprojection errors. In joint optimization tracking, a frame-to-model tracking method based on surface Gaussians is proposed to enhance tracking robustness by reducing the impact of artifacts and noise. Finally, we retain sparse feature point clouds for backend BA to reduce accumulated errors and lighten the computational burden on the device. Our main contributions are summarized as follows:

- We design an adaptive extended differentiable Gaussian method and rendering frame selection strategy based on a hybrid graph to achieve high-fidelity and compact scene representations.
- For tracking, we propose a joint optimization method based on surface Gaussians and sparse feature points to ensure accurate and robust frame-to-model tracking.
- We conducted experiments on different datasets, and the results demonstrate that our method outperforms the baseline in both tracking and mapping.

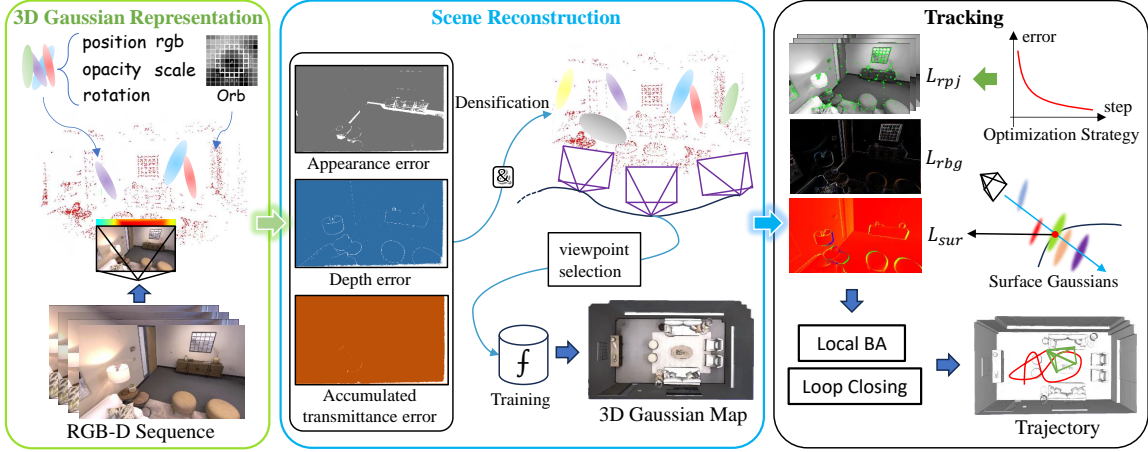


Fig. 1. In 3D Gaussian representation, RGB-D sequences are used as input. Gaussians are spawned to the scene based on the re-rendering of color, depth, and transmittance. A viewpoint selection strategy is used to choose the rendering frames for map training. Additionally, we not only tightly couple feature points and surface Gaussians but also perform lightweight global optimization through sparse point clouds, ultimately achieving accurate and robust tracking.

## II. RELATED WORK

### A. NeRF SLAM

NeRF [16] achieves realistic image rendering by performing pixel-ray sampling on 2D images. Utilizing multi-layer perceptron and volumetric differentiable rendering, NeRF can novel view synthesis of unobserved regions. iMAP [29] is the first to integrate NeRF into SLAM to achieve implicit neural representation. Since then, many excellent NeRF-based SLAM methods [33]–[35] have emerged. NICE-SLAM [30] proposes a hierarchical multi-feature grid to achieve high-quality scene reconstruction. Unlike iMAP, it updates only the visible grid features at each step. Orbeez-SLAM [31] uses ORB features for triangulation to implement monocular tracking with a depth-free estimator and employs NeRF for implicit scene representation. Point-SLAM [32] distributes point clouds onto object surfaces, which exhibits improved reconstruction quality through neural point cloud representation. However, NeRF ray sampling for individual pixels incurs high computational costs, leading to slow rendering speeds (below 15 FPS).

### B. 3DGS SLAM

Recently, 3D Gaussian Splatting (3DGS), which employs tile-based rasterization to render high-resolution images, has achieved significantly faster rendering speeds, reaching up to 300 FPS. Many researchers have attempted to integrate this advanced technology into SLAM [17], [18], [22], [23]. Splat-TAM [5] optimizes camera poses by minimizing photometric error through differentiable Gaussians guided by silhouettes and adds 3DGS to unobserved areas based on the geometric median depth error. Nevertheless, this methodology may result in an excessive number of Gaussian primitives, thereby markedly increasing the memory requirements and computational burden. Gaussian-SLAM [6] explores the limitations of 3DGS in SLAM and utilizes the submap to seed and optimize Gaussians, ultimately achieving camera pose tracking and map rendering. GS-SLAM [19] derives an analytical formula for backward optimization with re-rendering RGB-D loss

and uses depth filtering to remove unstable Gaussians during tracking. However, setting the appropriate depth filtering threshold is difficult, as it must account for noise and convergence levels. Photo-SLAM [20] employs feature points to determine camera poses and proposes a Gaussian-Pyramid-based training approach to construct scenes. Jiang [21] designs a method that connects ORB-SLAM3 with 3DGS, enabling a combination of those techniques. Although both Photo-SLAM [20] and Jiang [21] utilize feature points, they do not fully exploit the potential performance benefits of feature points. Through our analysis of 3DGS, we have found that feature points can significantly enhance 3DGS-SLAM in multiple aspects.

### C. Traditional SLAM

Traditional visual SLAM methods have evolved into two major categories: direct methods and feature methods. Direct methods [24], [25] estimate camera poses by minimizing photometric error and comparing pixel differences between two adjacent frames. This requires a strong assumption of photometric consistency. Feature methods [26], [27] use image features such as corners and lines. These methods minimize pixel errors between corresponding features across frames using reprojection error. The ORB-SLAM series [1], [10], [28] achieves real-time accurate localization based on ORB features and performs global optimization of sparse landmarks and poses through graph optimization. Although these methods excel in real-time performance and localization accuracy compared to advanced scene representation techniques (e.g., NeRF, 3DGS), their limited environment representation capabilities constrain their applicability to more advanced tasks.

## III. METHOD

The overview of our propose GSORB-SLAM system is shown in Fig. 1. Given a set of RGB-D sequences as input, we first introduce a 3D Gaussian field  $\mathbf{G}$  (III-A). Secondly, we propose a method to use Gaussians for incremental

mapping efficiently and how to select RF for training (III-B). Finally, we design the acquisition of surface Gaussians and how to achieve accurate and robust pose tracking by jointly using the ORB feature, along with lightweight global optimization based on sparse landmarks (III-C).

### A. 3D Gaussian field

**Gaussian map representation.** Our scene of SLAM is represented by a collection of anisotropic 3D Gaussian with opacity attributes:

$$\mathbf{G} = \{G_i : (X_i^w, \Sigma_i, o_i, c_i) | i = 1, \dots, N\}. \quad (1)$$

Similar to [4], each Gaussian contains a group of parameters: the position  $X_i^w \in \mathbb{R}^3$  in the world coordinate system, the opacity  $o_i \in [0, 1]$ , the trichromatic vector  $c_i \in \mathbb{R}^3$  representing the color of each Gaussian and the 3D covariance matrix  $\Sigma_i \in \mathbb{R}^{3 \times 3}$  is a combination of a rotation matrix  $R \in SO(3)$ , and a scale diagonal matrix  $S \in \mathbb{R}^{3 \times 3}$ .

$$\Sigma_i = RSS^T R^T. \quad (2)$$

**Differentiable rendering.** 3DGS renders colors by blending Gaussians along rays, from near to far, and splatting them onto the pixel screen.

$$\tilde{C} = \sum_{i=1}^n c_i \alpha_i T_i, T_i = \prod_{j=1}^{i-1} (1 - \alpha_j), \quad (3)$$

where the density  $\alpha_i$  denotes the opacity contribution of the Gaussian to the pixel, which is determined by both the Gaussian function and the opacity.  $T_i$  is the accumulated transmittance, which decays as the ray passes through the number of Gaussians. Meanwhile, to obtain geometric information, depth  $z$  in the camera coordinate system are used instead of color  $c$  for rendering:

$$\tilde{D} = \sum_{i=1}^n z_i \alpha_i T_i. \quad (4)$$

Inspired by [3], we impose constraints on  $T_i$  to obtain the surface depth:

$$\tilde{D}_s = \max\{z_i | T_i > 0.5\}. \quad (5)$$

Since the surface depth is selected based on the median of the accumulated transmittance, if the transmittance remains less than full transmittance (set to 1) even in a converged state, the surface depth will be uncertain. Therefore, we need to estimate the accumulated transmittance of the pixel to ensure that the obtained surface depth is stable.

$$\tilde{T} = \sum_{i=1}^n \alpha_i T_i. \quad (6)$$

### B. Mapping

**Initialization.** In SLAM, large-scale Gaussian primitives may occupy spatial regions, affecting the addition of new initialized Gaussian in under-reconstructed. To address this, it is advisable to initialize the Gaussian scale to be roughly the size of a single pixel [5], [6]. For the  $i$ -th Gaussian

initialization, the position  $X_i^w$  is determined by the 3D points  $X_i^c$  in the camera coordinate system and the extrinsic matrix  $W_{wc}$ , which represents the camera-to-world transformation. The color  $c_i$  is extracted from the RGB image, opacity is initialized to 1, and the  $R_i$  rotation matrix is initialized to the unit quaternion  $q \in SE(3)$ . The scale is initialized to the three-dimensional vector  $s_i \in \mathbb{R}^3$  as follows:

$$s_i = \frac{(KW_{wc}X_i^c)_z}{d_f}, d_f = \left| \frac{f_x + f_y}{2} \right|, \quad (7)$$

$K$  is the camera intrinsic matrix,  $(\cdot)_z$  takes the third dimension, which corresponds to depth.  $f$  is the camera focal length.

**Adaptive densification.** To improve the convergence speed of differentiable Gaussians and obtain high-fidelity results, it is important to spawn new Gaussians to model the geometry and appearance of newly observed areas. We design an appearance mask  $M_c$ , which is generated based on the grayscale values of the re-rendering image, and a reconstructed geometric mask  $M_d = (|D - \tilde{D}| < 0.05) (\tilde{D} > 0)$ .

Since the geometric accuracy of rendering is influenced by the convergence of differentiable Gaussians, we design an adaptive depth error threshold  $\sigma_d$  to prevent redundant additions:

$$\sigma_d = \mu\{E_d\} + 40\eta\{E_d\} \quad (8)$$

$$E_d = |D(x, y) - \tilde{D}(x, y)|_{(x, y) \in M_d} \quad (9)$$

$\mu\{\cdot\}$  is the mean operation,  $\eta\{\cdot\}$  is the median operation. Spawning new Gaussians needs to meet the following requirements:

(1) Based on accumulated transmittance:  $\tilde{T}(x, y) < 0.8$ . This helps to improve areas where gradient descent is slow due to a lack of supervision by re-initializing them. In SLAM, it is unfeasible to set a enough number of iterations for training. Another reason is to ensure tracking accuracy, a new Gaussian needs to be spawned if the accumulated transmittance has not reached 80% of the full transmittance.

(2) Based on geometry:  $(M_c < 50) (E_d < \sigma_d) (\tilde{T}(x, y) < 0.99)$ . The  $(M_c < 50) (E_d < \sigma_d)$  is to identify under-reconstructed areas by using errors in geometry and ap-

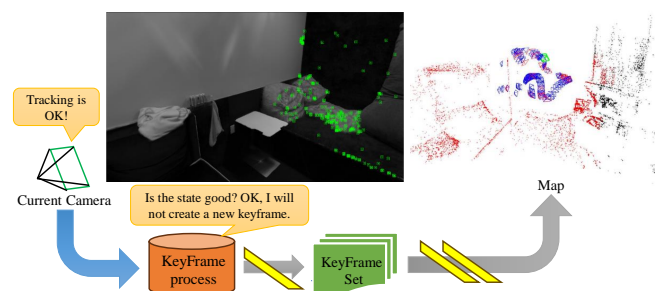


Fig. 2. The green points represent feature points. At this moment, a keyframe should be generated, but in this case, since the tracking requirements are met, a keyframe is not generated and inserted into the map. As a result, observations of this region will be lost during subsequent training.

pearance, while  $(\tilde{T}(x, y) < 0.99)$  is to prevent continuously adding Gaussians due to significant geometric errors at the edges. As illustrated in Fig. 1, the accumulated transmittance proves to be more robust against edge errors.

The new Gaussians will be spawned to regions that meet at least one of the above criteria:

$$Add(G_i), \text{ if (1) or (2).} \quad (10)$$

**Keyframe generation.** Feature-based SLAM [1] focuses only on the number of feature points and does not consider their distribution, shown in Fig. 2. Therefore, an overlap graph method is designed to generate keyframes based on the degree of overlap:

$$OG(i, j) = \frac{\pi(W_{ij}, \mathcal{K}_j)}{\mathcal{K}_i}, \quad (11)$$

where  $\pi_{ij}(\cdot)$  represents the projection of the  $j$ -th frame onto the  $i$ -th frame, and  $\mathcal{K}_i$  indicates the number of random points in the  $i$  frame.

**Rendering frame selection strategy.** The RF are selected from keyframes, and a good selection strategy can greatly improve rendering quality. The TAMBRIDGE [21] achieves excellent reconstruction results by selecting a keyframe based on the co-visibility graph [1]. However, we found that relying solely on the set of rendering frames selected from the co-visibility graph might lead to limitations in training perspectives, potentially only covering a small portion of the main object. These factors can lead to a decline in reconstruction quality. To address this, we propose a novel rendering frame selection strategy based on a hybrid graph.

First, we select the adjacency  $n_a$  frames and the optimized  $n_b$  frames to add to RF set  $\mathcal{R}$ . The adjacency frames increase the probability of the current viewpoint being selected, as the current viewpoint requires more optimization for tracking. Additionally, the optimized frames are included due to the presence of the backend pose optimization thread.

Secondly, a window  $W$  is initialized with the current frame  $f_1$ . To improve the efficiency and quality of selection, candidate frames  $F_c$  are prioritized from the co-visibility graph. If  $OG(f_{top(W)}, f_j) < \beta_1$ , then  $f_j$  ( $j \in F_c$ ) will be added to the window and also to  $\mathcal{R}$ , until  $F_c$  has been fully traversed. The  $top(\cdot)$  is the index of the newly added frame. The window  $W$  can prevent approximately identical viewpoints from the co-visibility graph from being repeatedly added, as weak tracking continuously generates new keyframes. Additionally, since some keyframes are not present in the co-visibility graph, candidate frames  $F_k$  will be selected by sorting the keyframes based on their timestamps. These  $F_k$  will then be added to  $\mathcal{R}$  according to the overlap graph  $OG(f_1, f_j)_{j \in F_k} > \beta_2$ . It is worth noting that the number of frames added in this part does not exceed  $n_s$ .

Finally,  $n_r$  frames are randomly selected and added to  $\mathcal{R}$ . This is done to prevent catastrophic forgetting of the global map due to continuous learning.

**Map optimization.** In frame-to-model tracking mode, map optimization is crucial. In continuous SLAM, we design a isotropic regularization loss to overcome anisotropic

influence (strip-shaped Gaussian primitives):

$$\mathcal{L}_{iso} = \frac{1}{N} \sum_{i=0}^N (\max\{s_i\} - \min\{s_i\} | s_i > \gamma), \quad (12)$$

and a scalar regularization:

$$\mathcal{L}_s = \sum_{i=0}^N (s_i - \gamma | s_i > \gamma), \gamma = 0.03 * \max\{(\mathbf{G})_z\}. \quad (13)$$

To make the media Gaussian fit the surface better, we design a surface depth loss:

$$\mathcal{L}_{sur} = |\tilde{D}_s - D|_1. \quad (14)$$

Meanwhile, the surface depth requires geometric depth for maintenance, so we add geometry supervision:

$$\mathcal{L}_d = |\tilde{D} - D|_1. \quad (15)$$

For color supervision, we combine L1 and SSIM [7] losses:

$$\mathcal{L}_{rgb} = \lambda |\tilde{C} - C|_1 + (1 - \lambda)(1 - SSIM(\tilde{C}, C)). \quad (16)$$

Final map optimization loss:

$$\mathcal{L}_{mapping} = \omega_1^m \mathcal{L}_{rgb} + \omega_2^m \mathcal{L}_d + \omega_3^m \mathcal{L}_{sur} + \omega_4^m (\mathcal{L}_{iso} + 2\mathcal{L}_s), \quad (17)$$

where  $\omega^m$  is a set of weights for mapping.

### C. Tracking

**Frame-to-model tracking.** We jointly optimize the photometric error based on 3DGS re-rendering and ground truth, as well as the reprojection error based on feature points, to obtain accurate poses. The reprojection loss:

$$\mathcal{L}_{rep} = \sum_{j \in \mathcal{M}} \sum_{i \in \mathcal{P}} \varphi(\|p_i - \pi(W_{cj}, P_i^j)\|_2), \quad (18)$$

where  $\mathcal{M}$  is the set of local keyframes,  $\mathcal{P}$  represents the matched features,  $p_i$  is the pixel observation in the image,  $W_{cj}$  is the pose of the  $j$ -th camera relative to the current camera and  $P_i^j$  is  $i$ -th 3D point of  $j$ -th camera, and  $\varphi$  represents the information matrix.

During the optimization process, to prevent incorrect feature point matches from impacting the reduction of total loss, we will remove outliers in advance, allowing the re-rendering loss item to become the primary component.

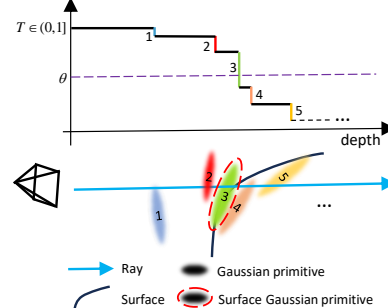


Fig. 3. Surface Gaussian analysis: The coordinate system represents the extent to which transmittance decreases after the ray passes through the Gaussian, along with a visualization of the corresponding position of the Gaussian. The value  $\theta$  is a predefined threshold, and the Gaussian where  $T$  drops to  $\theta$  indicates the depth value closest to the surface.

Since the re-rendering depth relies on accumulation from rays passing through Gaussians, it can exhibit instability. When a ray passes through a Gaussian with special opacity, the case represented by the index 1 in Fig. 3 or artifacts, this contribution will also be added to the final rendering result. Therefore, we propose surface depth instead of re-rendering depth to enhance the robustness of the tracking. Additionally, we only adopt Gaussian surfaces that are close to full transmittance as geometric features. Further, the optimize the combined loss using the Adam optimizer:

$$\mathcal{L}_{tracking} = (\tilde{T} > 0.99)(\omega_1^t \mathcal{L}_{rgb} + \omega_2^t \mathcal{L}_{sur}) + \omega_3^t \mathcal{L}_{rpb}. \quad (19)$$

**Bundle adjustment.** In the backend thread, we use graph optimization to jointly optimize map points and camera poses based on sparse feature points, similar to [1]. The backend operates as an independent thread, unaffected by the training. Therefore, once the camera poses are optimized, they can promptly provide more accurate camera poses for reconstruction, enhancing the reconstruction quality.

#### IV. EXPERIMENT

##### A. Experiment Setup

**Dataset.** To thoroughly evaluate the performance of the method presented in this paper, following [5], [30], [32], we select three sequences from the real-world TUM dataset [40] and eight sequences from the synthetic Replica [39] dataset for comprehensive evaluation.

**Baseline.** We select the state-of-the-art NeRF SLAM methods: NICE-SLAM [30] and Point-SLAM [32]. In addition, we include 3DGS-based SLAM methods: SplatTAM [5], GS-SLAM [19], MonoGS [18], Sun [37] and methods combining feature points and 3DGS: Photo-SLAM [20] and TANBRIDGE [21]. We also incorporated the traditional SLAM method: ORB-SLAM2 [1].

**Metrics.** For measuring RGB rendering performance we use PSNR(dB), SSIM and LPIPS. For camera pose estimation tracking we use the average absolute trajectory error (ATE RMSE [cm]) [38]. The **best** results will be highlighted in red, while the **second-best** will be highlighted in blue. The result is the average of six times data.

**Implementation details.** We fully compile our SLAM in C++ and CUDA. Additionally, the SLAM runs on a desktop

TABLE I

TRACKING RESULTS ON RGB-D TUM DATASET (ATE RMSE $\downarrow$  [CM]).  
"–" INDICATES UNAVAILABLE DATA BECAUSE THE RELATED WORK IS

NOT OPEN.

Method	Fr1/desk1	Fr2/xyz	Fr3/office	Avg.
ORB-SLAM2	1.60	0.40	<b>1.00</b>	<b>1.00</b>
Point-SLAM	4.34	1.31	3.48	3.04
NICE-SLAM	4.26	31.73	3.87	13.28
MonoGS(RGB-D)	<b>1.52</b>	1.58	1.65	1.58
GS-SLAM	3.30	1.30	6.60	3.73
SplatTAM	3.35	1.24	5.16	3.25
Sun	3.38	–	5.12	–
Photo-SLAM	2.60	<b>0.35</b>	1.00	1.31
TANBRIDGE	1.75	<b>0.32</b>	1.42	1.16
Ours	<b>1.48</b>	0.39	<b>0.88</b>	<b>0.91</b>

TABLE II  
TRACKING RESULTS ON THE REPLICA DATASET (ATE RMSE $\downarrow$  [CM]).  
THE LOST INDICATES TRACKING LOST.

Method	R0	R1	R2	Of0	Of1	Of2	Of3	Of4
ORB-SLAM2	0.45	<b>0.29</b>	Lost	0.47	0.28	0.75	0.69	0.59
Point-SLAM	0.61	0.41	0.37	<b>0.38</b>	0.48	0.54	0.69	0.72
NICE-SLAM	0.97	1.31	1.07	0.88	1.00	1.06	1.10	1.13
MonoGS(RGB-D)	0.47	0.43	0.31	0.70	0.57	<b>0.31</b>	<b>0.31</b>	3.20
GS-SLAM	0.48	0.53	0.33	0.52	0.41	0.59	0.46	0.70
SplatTAM	<b>0.31</b>	0.40	<b>0.29</b>	0.47	<b>0.27</b>	<b>0.29</b>	<b>0.32</b>	<b>0.55</b>
Ours	<b>0.35</b>	<b>0.22</b>	<b>0.33</b>	<b>0.33</b>	<b>0.19</b>	0.54	0.63	<b>0.45</b>

equipped with Intel i7-12700KF and an NVIDIA RTX 4060ti GPU. We set parameters  $\omega^m = \{1.0, 0.7, 0.1, 5\}$ ,  $\lambda = 0.8$   $\{\beta_1, \beta_2\} = \{0.07, 0.3\}$ ,  $\{n_a, n_b, n_s, n_r\} = \{5, 5, 13, 7\}$ . For the TUM datasets, we set weight  $\omega^t = \{1.0, 0.7, 0.1\}$ , and we set weight  $\omega^t = \{0.7, 1.0, 0.1\}$  for the Replica datasets.

##### B. Localization and Rendering Quality Evaluation

**Localization.** Table I shows the tracking results on the TUM RGB-D dataset. Our method outperforms other baseline methods, even surpassing the state-of-the-art ORB-SLAM2. In comparison, both TANBRIDGE and Photo-SLAM, which are based on ORBSLAM3 [10], exhibit general localization performance, while ours demonstrates superior localization accuracy. This is not only because we jointly optimize feature points and 3DGS, but also because we propose a novel surface geometry-based tracking method, which better handles noise in real-world environments. Table II reports results on the synthetic Replica dataset. The feature-based ORB-SLAM2 loses track in sequence R2, which contains a weakly textured wall. In contrast, our method not only achieves tracking across all sequences better than ORB-SLAM2, but it also outperforms other 3DGS-based SLAM methods.

**Rendering quality.** We quantitatively evaluate the rendering quality on the Replica and TUM RGB-D datasets, with the results shown in Table IV and Table V, respectively. It is evident that our method achieves superior rendering quality compared to others. The visualization results in Fig. 4 show that our method is capable of generating higher-quality realistic images.

##### C. Ablation Study

To demonstrate the role of our component within the GSORB-SLAM, we conducted a series of ablation experiments, with the results presented in Table III and Table VI. In Table VI, we analyse two typical sequences, but this does not mean that our method is ineffective on other sequences.

**Surface Depth vs. Depth.** We choose the TUM dataset because it contains noise from real-world environments, which strongly demonstrates the advantages of our method. As

TABLE III  
TRACKING RESULTS AT DIFFERENT DEPTHS ON THE TUM DATASETS.  
(ATE RMSE $\downarrow$  [CM])

Method	Fr1/desk1	Fr2/xyz	Fr3/office	Tracking/Iter.(ms)
Depth	2.46	0.41	0.94	16
Surface depth (Ours)	<b>1.48</b>	<b>0.39</b>	<b>0.88</b>	<b>11</b>

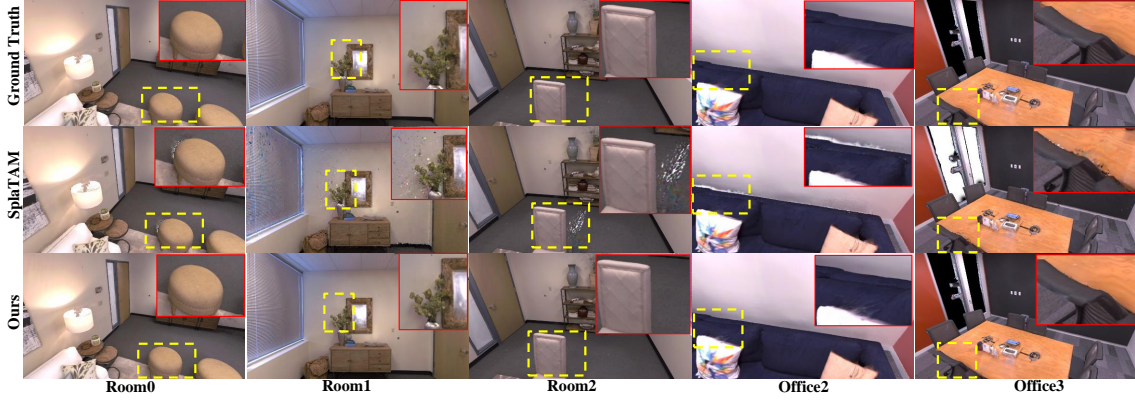


Fig. 4. The render visualization results on the Replica dataset.

TABLE IV

RENDERING PERFORMANCE COMPARISON OF RGB-D SLAM METHODS ON REPLIC A.

Sequence	Metric	R0	R1	R2	Of0	Of1	Of2	Of3	Of4
Point-SLAM	PSNR↑	32.40	34.80	35.50	38.26	39.16	33.99	33.48	33.49
	SSIM↑	0.97	<b>0.98</b>	0.98	0.98	0.99	0.96	0.96	<b>0.98</b>
	LPIPS↓	0.11	0.12	0.11	0.10	0.12	0.16	0.13	0.14
NICE-SLAM	PSNR↑	22.12	22.47	24.52	29.07	30.34	19.66	22.23	24.49
	SSIM↑	0.69	0.76	0.81	0.87	0.89	0.80	0.80	0.86
	LPIPS↓	0.33	0.27	0.21	0.23	0.18	0.24	0.21	0.20
SplatTAM	PSNR↑	32.86	33.89	35.25	38.26	39.17	31.97	29.70	31.81
	SSIM↑	<b>0.98</b>	0.97	<b>0.98</b>	0.98	0.98	0.97	0.95	0.95
	LPIPS↓	0.07	0.10	0.08	0.09	0.09	0.10	0.12	0.15
GS-SLAM	PSNR↑	31.56	32.86	32.59	38.70	41.17	32.36	32.03	32.92
	SSIM↑	0.968	0.973	0.971	0.986	<b>0.993</b>	<b>0.978</b>	<b>0.970</b>	0.968
	LPIPS↓	0.094	<b>0.075</b>	0.093	<b>0.050</b>	<b>0.033</b>	0.094	0.110	0.112
MonoGS(RGB-D)	PSNR↑	<b>34.83</b>	<b>36.43</b>	<b>37.49</b>	<b>39.95</b>	<b>42.09</b>	<b>36.24</b>	<b>36.70</b>	<b>36.07</b>
	SSIM↑	0.954	0.959	0.965	<b>0.971</b>	0.977	0.964	0.963	0.957
	LPIPS↓	<b>0.068</b>	0.076	<b>0.075</b>	0.072	0.055	<b>0.078</b>	<b>0.065</b>	<b>0.099</b>
Ours	PSNR↑	<b>35.58</b>	<b>38.07</b>	<b>38.60</b>	<b>42.09</b>	<b>42.49</b>	<b>36.63</b>	<b>36.06</b>	<b>37.89</b>
	SSIM↑	<b>0.986</b>	<b>0.990</b>	<b>0.992</b>	<b>0.993</b>	<b>0.993</b>	<b>0.988</b>	<b>0.989</b>	<b>0.989</b>
	LPIPS↓	<b>0.037</b>	<b>0.039</b>	<b>0.038</b>	<b>0.034</b>	<b>0.030</b>	<b>0.050</b>	<b>0.041</b>	<b>0.053</b>

shown in Table III, it is obvious that our method outperforms the tracking method based on re-rendering depth. This is because our method reduces the impact of artifacts and noise on tracking. In addition, our surface-based method is approximately 10ms faster than the re-rendering-based method.

**RF selection strategy.** To ensure meaningful comparisons, we reference the frame selection method used in TANBRIDGE, which is based on a co-visibility selection strategy. As shown in Table VI, our method not only improves rendering quality but also enhances localization accuracy.

**Keyframe generation.** To demonstrate that generating keyframes based on sparse feature points has deficiencies in constructing 3D Gaussian fields, similar to what is proposed in TANBRIDGE, we compare original keyframes generated [1] from feature points with our method. In Table VI, our method shows improvements in both PSNR 3 dB and ATE 0.29 cm. Especially in the Of1 sequence, the presence of mostly weak textures prevents keyframes generation, affecting the sampling during training.

TABLE V

RENDERING PERFORMANCE COMPARISON OF RGB-D SLAM METHODS ON TUM DATASETS. “–” INDICATES UNAVAILABLE DATA BECAUSE THE RELATED WORK IS NOT OPEN.

Sequence	Metric	Fr1/desk1	Fr2/xyz	Fr3/office
Point-SLAM	PSNR↑	13.87	17.56	18.43
	SSIM↑	0.63	0.71	0.75
	LPIPS↓	0.54	0.59	0.45
NICE-SLAM	PSNR↑	12.00	18.20	16.34
	SSIM↑	0.42	0.60	0.55
	LPIPS↓	0.51	0.31	0.39
TANBRIDGE	PSNR↑	21.22	23.44	20.15
	SSIM↑	0.88	0.90	0.82
	LPIPS↓	0.19	<b>0.10</b>	0.25
Photo-SLAM	PSNR↑	20.870	22.094	<b>22.744</b>
	SSIM↑	0.743	0.765	0.780
	LPIPS↓	0.239	0.169	<b>0.154</b>
Sun	PSNR↑	<b>22.60</b>	–	22.30
	SSIM↑	<b>0.91</b>	–	<b>0.89</b>
	LPIPS↓	<b>0.15</b>	–	<b>0.16</b>
SplatTAM	PSNR↑	22.00	<b>24.50</b>	21.90
	SSIM↑	0.86	<b>0.95</b>	0.88
	LPIPS↓	0.19	0.10	0.20
Ours	PSNR↑	<b>23.10</b>	<b>24.70</b>	<b>24.38</b>
	SSIM↑	<b>0.886</b>	<b>0.936</b>	<b>0.911</b>
	LPIPS↓	<b>0.176</b>	<b>0.114</b>	0.171

TABLE VI

THE ABLATION ANALYSIS ON REPLICA R0 AND OF1 SEQUENCES.

RF Stra.	KF Gen.	Reg.	R0		Of1	
			ATE ↓	PSNR ↑	ATE ↓	PSNR ↑
✓	✓	✓	<b>0.35</b>	<b>35.58</b>	<b>0.19</b>	<b>42.49</b>
✗	✓	✓	0.35	34.24	0.24	41.51
✓	✗	✓	0.38	35.21	0.76	35.43
✓	✓	✗	0.37	35.52	0.20	42.10

**Regularization.** In Table VI, the regularization plays a certain role. This is because the regularization suppresses the Gaussian from forming elongated shapes, thereby reducing its impact on localization.

## V. CONCLUSION

We proposed GSORB-SLAM, a tightly coupled system integrating 3DGs and ORB features. Experimental results demonstrated that our joint optimization method, based on geometric surfaces and feature points, reduced the sensitivity of the system to noise. The viewpoint selection strategy, based on a hybrid graph, and the adaptive Gaussian expansion method were designed to improve the rendering quality of dense SLAM. Through experiments, our approach showed impressive performance.

## REFERENCES

[1] Mur-Artal R, Tardós J D. Orb-slam2: An open-source slam system for monocular, stereo, and rgbd cameras[J]. *IEEE transactions on robotics*, 2017, 33(5): 1255-1262.

[2] Kümmerle R, Grisetti G, Strasdat H, et al. g 2 o: A general framework for graph optimization[C] 2011 IEEE international conference on robotics and automation. IEEE, 2011: 3607-3613.

[3] Huang B, Yu Z, Chen A, et al. 2d gaussian splatting for geometrically accurate radiance fields[C] ACM SIGGRAPH 2024 Conference Papers. 2024: 1-11.

[4] Kerbl B, Kopanas G, Leimkühler T, et al. 3D Gaussian Splatting for Real-Time Radiance Field Rendering[J]. *ACM Trans. Graph.*, 2023, 42(4): 139:1-139:14.

[5] Keetha N, Karhade J, Jatavallabhula K M, et al. SplaTAM: Splat Track & Map 3D Gaussians for Dense RGB-D SLAM[C] Proceedings of the IEEE/CVF Conference on Computer Vision and Pattern Recognition. 2024: 21357-21366.

[6] Yugay V, Li Y, Gevers T, et al. Gaussian-slam: Photo-realistic dense slam with gaussian splatting[J]. *arXiv preprint arXiv:2312.10070*, 2023.

[7] Wang Z, Bovik A C, Sheikh H R, et al. Image quality assessment: from error visibility to structural similarity[J]. *IEEE transactions on image processing*, 2004, 13(4): 600-612.

[8] Stückler J, Behnke S. Multi-resolution surfel maps for efficient dense 3D modeling and tracking[J]. *Journal of Visual Communication and Image Representation*, 2014, 25(1): 137-147.

[9] Whelan T, Leutenegger S, Salas-Moreno R F, et al. ElasticFusion: Dense SLAM without a pose graph[C] *Robotics: science and systems*. 2015, 11: 3.

[10] Campos C, Elvira R, Rodríguez J J G, et al. Orb-slam3: An accurate open-source library for visual, visual-inertial, and multimap slam[J]. *IEEE Transactions on Robotics*, 2021, 37(6): 1874-1890.

[11] Schöps T, Sattler T, Pollefeys M. Surfelmeshing: Online surfel-based mesh reconstruction[J]. *IEEE transactions on pattern analysis and machine intelligence*, 2019, 42(10): 2494-2507.

[12] Ruetz F, Hernández E, Pfeiffer M, et al. Ovpc mesh: 3d free-space representation for local ground vehicle navigation[C] 2019 International Conference on Robotics and Automation (ICRA). IEEE, 2019: 8648-8654.

[13] Maier R, Schaller R, Cremers D. Efficient online surface correction for real-time large-scale 3D reconstruction[J]. *arXiv preprint arXiv:1709.03763*, 2017.

[14] Newcombe R A, Izadi S, Hilliges O, et al. Kinectfusion: Real-time dense surface mapping and tracking[C] 2011 10th IEEE international symposium on mixed and augmented reality. Ieee, 2011: 127-136.

[15] Duan J, Yu S, Tan H L, et al. A survey of embodied ai: From simulators to research tasks[J]. *IEEE Transactions on Emerging Topics in Computational Intelligence*, 2022, 6(2): 230-244.

[16] Mildenhall B, Srinivasan P P, Tancik M, et al. Nerf: Representing scenes as neural radiance fields for view synthesis[J]. *Communications of the ACM*, 2021, 65(1): 99-106.

[17] Li M, Liu S, Zhou H. Sgs-slam: Semantic gaussian splatting for neural dense slam[J]. *arXiv preprint arXiv:2402.03246*, 2024.

[18] Matsuki H, Murai R, Kelly P H J, et al. Gaussian splatting slam[C] Proceedings of the IEEE/CVF Conference on Computer Vision and Pattern Recognition. 2024: 18039-18048.

[19] Yan C, Qu D, Xu D, et al. Gs-slam: Dense visual slam with 3d gaussian splatting[C] Proceedings of the IEEE/CVF Conference on Computer Vision and Pattern Recognition. 2024: 19595-19604.

[20] Huang H, Li L, Cheng H, et al. Photo-SLAM: Real-time Simultaneous Localization and Photorealistic Mapping for Monocular Stereo and RGB-D Cameras[C] Proceedings of the IEEE/CVF Conference on Computer Vision and Pattern Recognition. 2024: 21584-21593.

[21] Jiang P, Liu H, Li X, et al. TAMBRIDGE: Bridging Frame-Centered Tracking and 3D Gaussian Splatting for Enhanced SLAM[J]. *arXiv preprint arXiv:2405.19614*, 2024.

[22] Hu J, Chen X, Feng B, et al. CG-SLAM: Efficient Dense RGB-D SLAM in a Consistent Uncertainty-aware 3D Gaussian Field[J]. *arXiv preprint arXiv:2403.16095*, 2024.

[23] Li M, Huang J, Sun L, et al. NGM-SLAM: Gaussian Splatting SLAM with Radiance Field Submap[J]. *arXiv preprint arXiv:2405.05702*, 2024.

[24] Wang R, Schworer M, Cremers D. Stereo DSO: Large-scale direct sparse visual odometry with stereo cameras[C] Proceedings of the IEEE international conference on computer vision. 2017: 3903-3911.

[25] Engel J, Schöps T, Cremers D. LSD-SLAM: Large-scale direct monocular SLAM[C] European conference on computer vision. Cham: Springer International Publishing, 2014: 834-849.

[26] Davison A J, Reid I D, Molton N D, et al. MonoSLAM: Real-time single camera SLAM[J]. *IEEE transactions on pattern analysis and machine intelligence*, 2007, 29(6): 1052-1067.

[27] Gomez-Ojeda R, Moreno F A, Zuniga-Noél D, et al. PL-SLAM: A stereo SLAM system through the combination of points and line segments[J]. *IEEE Transactions on Robotics*, 2019, 35(3): 734-746.

[28] Mur-Artal R, Montiel J M M, Tardos J D. ORB-SLAM: a versatile and accurate monocular SLAM system[J]. *IEEE transactions on robotics*, 2015, 31(5): 1147-1163.

[29] Sucar E, Liu S, Ortiz J, et al. imap: Implicit mapping and positioning in real-time[C] Proceedings of the IEEE/CVF international conference on computer vision. 2021: 6229-6238.

[30] Zhu Z, Peng S, Larsson V, et al. Nice-slam: Neural implicit scalable encoding for slam[C] Proceedings of the IEEE/CVF conference on computer vision and pattern recognition. 2022: 12786-12796.

[31] Chung C M, Tseng Y C, Hsu Y C, et al. Orbeez-slam: A real-time monocular visual slam with orb features and nerf-realized mapping[C] 2023 IEEE International Conference on Robotics and Automation (ICRA). IEEE, 2023: 9400-9406.

[32] Sandström E, Li Y, Van Gool L, et al. Point-slam: Dense neural point cloud-based slam[C] Proceedings of the IEEE/CVF International Conference on Computer Vision. 2023: 18433-18444.

[33] Johari M M, Carta C, Fleuret F. Eslam: Efficient dense slam system based on hybrid representation of signed distance fields[C] Proceedings of the IEEE/CVF Conference on Computer Vision and Pattern Recognition. 2023: 17408-17419.

[34] Wang H, Wang J, Agapito L. Co-slam: Joint coordinate and sparse parametric encodings for neural real-time slam[C] Proceedings of the IEEE/CVF Conference on Computer Vision and Pattern Recognition. 2023: 13293-13302.

[35] Sandström E, Ta K, Van Gool L, et al. Uncle-slam: Uncertainty learning for dense neural slam[C] Proceedings of the IEEE/CVF International Conference on Computer Vision. 2023: 4537-4548.

[36] Luiten J, Kopanas G, Leibe B, et al. Dynamic 3d gaussians: Tracking by persistent dynamic view synthesis[J]. *arXiv preprint arXiv:2308.09713*, 2023.

[37] Sun S, Mielle M, Lilienthal A J, et al. High-Fidelity SLAM Using Gaussian Splatting with Rendering-Guided Densification and Regularized Optimization[J]. *arXiv preprint arXiv:2403.12535*, 2024.

[38] Sturm J, Engelhard N, Endres F, et al. A benchmark for the evaluation of RGB-D SLAM systems[C] 2012 IEEE/RSJ international conference on intelligent robots and systems. IEEE, 2012: 573-580.

[39] Straub J, Whelan T, Ma L, et al. The Replica dataset: A digital replica of indoor spaces[J]. *arXiv preprint arXiv:1906.05797*, 2019.

[40] Sturm J, Engelhard N, Endres F, et al. A benchmark for the evaluation of RGB-D SLAM systems[C] 2012 IEEE/RSJ international conference on intelligent robots and systems. IEEE, 2012: 573-580.